Microwave-assisted esterification of bleached and unbleached cellulose nanofibers

Farida Baraka, Eduardo Robles, Jalel Labidi

Industrial Crops & Products 191 (2023) 115970

Contents lists available at ScienceDirect

Industrial Crops & Products

journal homepage: www.elsevier.com/locate/indcrop

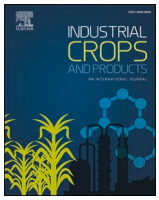

Microwave-assisted esterification of bleached and unbleached cellulose nanofibers

Farida Baraka [a], Eduardo Robles [b], Jalel Labidi [a,*]

[a] Biorefinery Processes Group, Chemical and Environmental Engineering Department, Engineering Faculty of Gipuzkoa, University of the Basque Country UPV/EHU, Plaza Europa 1, 20018 Donostia, Spain

[b] University of Pau and the Adour Region, E2S UPPA, CNRS, Institute of Analytical and Physicochemical Sciences for the Environment and Materials (IPREM-UMR 5254), 403 Rue de Saint Pierre, 40004 Mont de Marsan, France

ARTICLE INFO

Keywords:
Cellulose nanofibers
Extraction
Esterification
Microwave
Aromatic amine

ABSTRACT

Microwave-assisted synthetic pathway was explored for the sustainable esterification of cellulose nanofibers (CNFs) using an aromatic amine compound. For this purpose, nanofibers were isolated from unbleached and bleached eucalyptus pulp through the homogenization process. The chemical composition, the structural properties, the morphology, and the thermal properties of the extracted nanofibers were investigated. *para*-aminobenzoic acid (PABA) was employed to esterify CNFs's aliphatic hydroxyl groups. FTIR and ^{13}C NMR spectroscopy confirmed the success of the chemical modification. The structural characterization of the cellulose nanofibers and lignocellulose nanofibrils esterified (CNF-E and LCNF-E) confirmed the grafting of the aromatic amine counterparts onto CNFs's surface. The thermogravimetric technique assessed the thermal stability of the nanofibrils. The thermal properties were affected by the esterification resulting in a significant improvement of the char yield (CR) compared to the original CNFs (from CR≈ 10% to > 20%). Finally, this sustainable chemical pathway increases CNFs's functionality by introducing ester and aromatic amine functionalities, making LCNF-E and CNF-E sustainable platforms for further smart applications.

1. Introduction

Given the considerable attention and efforts to reduce climate change, actions are shifting from the current fossil fuel-based economy to a more sustainable economy based on renewable energy, biomass, and recycling. Stemming from their abundance, biodegradability, robust mechanical properties, and tunable surface chemistry (Moon et al., 2011), nanocellulose has been pointed out as a great deal of interest to drive this transition (Eichhorn et al., 2010). Nanocellulose is a biopolymer composed of a crystalline fibrous structure embedded in an amorphous matrix of lignin, pectin, and hemicellulose (Chang et al., 2019). It is classified into (1) cellulose nanofibers (CNFs) and (2) cellulose nanocrystals (CNCs) according to the morphology obtained after its isolation from the plant source. CNCs are rod-like crystalline fragments of cellulose from which amorphous regions are selectively removed through acid hydrolysis (Chang et al., 2019). CNFs are filamentous fragments that contain both amorphous and crystalline domains (Yuan et al., 2021).

CNFs can be isolated from different sources of lignocellulosic biomass, such as wood fibers or annual plants. Over the years, several methods have been explored to extract CNFs from the lignocellulosic biomass, including mechanical processes such as high-pressure homogenization (HPH) (Herrick et al., 1983; Turbak et al., 1983), microfluidization (Li et al., 2014; Xiang et al., 2016), grinding (Nair et al., 2014; Vartiainen et al., 2011), and ultrasonication (Li et al., 2013; Wang et al., 2015). In general, CNFs production from plant biomass starts with a treatment to partially or entirely remove matrix components such as lignin and hemicellulose. Then, the pulping and multistage bleaching process aims to separate it from the fiber to ultimately promote CNFs individualization and accessibility (Oliveira et al., 2006). However,

Abbreviations: -OH, hydroxyl; CNFs, cellulose nanofibers; CNCs, cellulose nanocrystals; LCNF, lignocellulose nanofibrils; H_2SO_4, sulfuric acid; PABA, *para*-aminobenzoic acid; SEM, scanning electron microscopy; AFM, atomic force microscopy; XRD, X-ray diffraction; TGA, thermogravimetric analysis; DSC, differential scanning calorimetry; FTIR, Fourier transform infrared spectroscopy; NMR, nuclear magnetic resonance; MW, microwave; IC, crystallinity index; T_m, melting temperature; ΔH_m, melting enthalpy.

* Corresponding author.
E-mail addresses: farida.baraka@ehu.eus (F. Baraka), eduardo.robles@univ-pau.fr (E. Robles), jalel.labidi@ehu.eus (J. Labidi).

https://doi.org/10.1016/j.indcrop.2022.115970
Received 25 July 2022; Received in revised form 2 November 2022; Accepted 10 November 2022
Available online 23 November 2022

lignin biopolymer, responsible for the hardness and resistance of the lignocellulosic plant cell walls, may modify the polarity and the hydrophilicity of CNFs due to its low water interaction (Bian et al., 2018). Several studies have reported that unbleached nanofibers containing residual lignin (LCNFs) demonstrate interesting features such as high yield, low production cost, low environmental impact, and improved drainage (Spence et al., 2010; Rojo et al., 2015; Demuner et al., 2020).

CNFs provide many hydroxyl groups on their surface, which confers a complex network supported by numerous hydrogen bonds. These interactions are responsible for the crystalline structure, making CNFs insoluble in water and organic solvents at room temperature (Yuan et al., 2021). This enriched surface stands for a breeding ground for developing functional materials to meet the growing demand for ecological products (Missoum et al., 2013). Various surface modifications have been reported, such as esterification (Aloulou et al., 2006), etherification (Eyholzer et al., 2012), oxidation (Nooy et al., 2010), silylation (Robles et al., 2018), and polymer grafting (Lönnberg et al., 2008), allowing a wide range of applications (Menon et al., 2017).

Esterification is one of the leading chemical modification techniques that has been widely used to modify cellulose structure (Missoum et al., 2013). This latter is a reaction in which an acylating agent reacts with the hydroxyl groups of cellulose nanofibers to produce ester groups. Acid anhydrides (Aloulou et al., 2006), acyl chlorides (Chhajed et al., 2019), or carboxylic acid (Ramírez et al., 2014) were used to esterify CNFs surface in order to achieve the required properties for the desired application. Sehaqui *et al.* have reported the preparation of a wide carboxyl-functionalized CNF via the esterification of wheat fibers with various cyclic anhydrides (maleic, phthalic, and succinic), leading to esterified CNFs with better thermal stability (Sehaqui et al., 2016). In the case of the esterification using acyl chlorides reagents, Chhajed *et al.* have developed a highly porous super hydrophobic CNFs synthesized from stearic acid chloride and found to be highly selective as a superabsorbent for oils and organic pollutants (Chhajed et al., 2019). Her *et al.* have recently conducted a study on the surface modification of CNFs using valeric or hexanoic acid (Her et al., 2020). Due to the freshly grafted alkyl side chains , these esterified CNFs show higher hydrophobicity enabling their dispersion in nonpolar organic media.

The surface modification of CNFs usually involves complicated and lengthy procedures or hazardous chemicals, hindering its large-scale production and limiting the sphere of application (Bouhdadi et al., 2011). Recently, an economically and environmentally sustainable CNFs esterification process operated under microwave (MW) energy has been reported to reduce reaction time. The principle behind MW heating is based on the polar characteristic of molecules and their ability to absorb and transform microwave radiation into heat. The MW heating process proved to be efficient, simple, clean, and solvent-free. For example, Joly *et al.* have reported the esterification of cellulose with acyl chloride derivatives by MW irradiation, where the reaction time was reduced from several hours to only 30 min (Joly et al., 2002). Similarly, Semsarilar *et al.* have investigated the dissolution and the functionalization of cellulose in the DMAc/LiCl system assisted by MW irradiation (Semsarilar and Perrier, 2009). They demonstrated a time-saving method allowing the esterification in a single step. More recently, Ragab *et al.* have evaluated the effects of CNFs esterification with acetic anhydride under MW irradiation onto several product's properties such as the surface area and the particle size distribution (Ragab and El Nemr, 2018). Esterification of cellulose nanofibers reported so far focus on the introduction of aliphatic moieties by harmful, long and expensive synthetic pathways. An innovative approach would be to graft aromatic amines through a sustainable, time saving, and cost efficient method. Thus, the elaboration of esterified and aromatic-amines based CNFs will enhance the thermal and mechanical stability certainly beneficial for further applications such as wastewater treatment, antimicrobial films, carbon adsorbents, or even key-precursor for subsequent chemical modifications. Besides, the hydrophobic character of aromatic compounds could be interesting for the elaboration of nanocomposites with apolar polymer systems, which can also exhibit barrier properties.

The current work aims to develop an efficient and green method for the introduction of aromatic molecules on the surface of CNFs extracted from the eucalyptus pulp. First, standard TAPPI methods were used to determine the chemical composition of the eucalyptus cellulosic pulp used in this research work, including extractible, ash, lignin, cellulose, and hemicelluloses. Then, CNFs were isolated from unbleached and bleached pulps by the homogenization process. Later, functional cellulose was prepared by the MW-assisted esterification of the extracted CNFs with *para*-aminobenzoic acid (PABA) . PABA is an aromatic carboxylic acid biologically produced from glucose, classified as a non-toxic and readily biodegradable reagent allowing its use in dyes and food additives. Finally, the aromatic amine function grafted onto the CNFs surface by MW-assisted esterification might open new possibilities for producing and applying eco-materials from nanocelluloses.

2. Experimental methods

2.1. Materials

A local producer kindly provided bleached and unbleached cellulose pulps extracted from *Eucalyptus* sp. in their wet form (Papelera Guipuzcoana de Zicuñaga). All chemicals, including toluene, sulfuric acid, and *para*-aminobenzoic acid, were purchased from Sigma-Aldrich as reagent grade and used as received without any further purification.

2.2. Chemical composition of the selected biomass

The analysis of the chemical composition of Eucalyptus cellulose pulps employed in this work includes the quantification of extractives, lignin, cellulose, hemicelluloses, and ash. The lignin content was determined using a gravimetric method in compliance with the standard TAPPI T222 method , following the removal of extractives according to the standard TAPPI T204 method . Next, the content of holocellulose was determined according to the TAPPI Useful Method 249. Subsequent, the content of hemicelluloses was calculated as the delta between the holocellulose and cellulose contents. Finally, ash content was determined by a gravimetric method in compliance with standard TAPPI T211 (Ash in Pulp combustion at 525 °C). All chemical analyses were performed in triplicate for each pulp.

2.3. Mechanical defibrillation of cellulose and lignocellulose

In order to obtain CNF and LCNF, the pulp fibers were subjected to a homogenization process. For this purpose, wet cellulose pulps (bleached and unbleached) were dispersed in water to reach a final concentration of 10 wt.%, subsequently introduced into an Ultraturrax high shear homogenizer, in which the fibers were kept at 20 000 rpm for 15 min. Later, the fibers were defibrillated using a GEA Niro Soavi high-pressure homogenizer. For this, 20 cycles were carried out with a starting pressure of 100 bar and increased up to a maximum of 600 bar with a flow rate of 10 L/h.

2.4. Preparation of CNF and LCNF prior to modification

Before esterification, the bleached and unbleached nanofibers solutions were freeze-dried to eliminate water through sublimation. To this aim, 10 g of each pulp containing 1 wt.% CNFs in water were cast into polystyrene Petri dishes and frozen at – 4 °C overnight. The films from different samples were prepared simultaneously so that the freezing conditions could be considered as similar. The freeze-drying was done inside a vacuum freeze dryer Coolsafe at a condenser temperature of – 110 °C at reduced pressure during 72 h. The collected porous samples were self-standing, lightweight, and soft. The resulting materials were then processed into powder form. For this, the foam samples were ground into a fine powder using an ultra-centrifugal mill (Retsch ZM

200, 6000 rpm, ϕ < 40 μm). The resulting nanofibers were then dried at 50 °C for 48 h.

2.5. Surface esterification of cellulose nanofibers

The cellulose nanofibers were esterified under vigorous stirring and microwave irradiations (flexiWAVE, Milestone, Sorisole, Italy) in the presence of toluene and sulfuric acid (H_2SO_4) (5% diluted solution) as reported in Scheme 1 following a previously reported protocol (Singh et al., 2016). Toluene was used to restrict the reactants to enter the bulk sites of fibers, thereby promoting the esterification of surface sites and keeping the crystalline core intact. H_2SO_4 was used as a catalyst to increase the rate of esterification. For the esterification, the ratio of 4-amino-benzoic acid (*para*-amino-benzoic acid, PABA) to fibers was fixed at 2:1 (wt./wt.). After stirring, the Quartz cup was tightly closed, and the reaction crude was placed into the microwave oven, where the mixture was heated up to 80 °C for 15 min at a microwave power of 300 W. When the reaction was completed, the Quartz cup was removed from the microwave and then cooled to room temperature. Next, the mixture was transferred to a flask where the toluene was evaporated under reduced pressure. Subsequently, an appropriate amount of ethanol was added to the flask and stirred for several minutes to solubilize the excess of unreacted PABA and filtered with a Büchner funnel. Finally, the product was dried at 50 °C for 48 h and then analyzed.

2.6. Characterization

2.6.1. Scanning electron microscopy (SEM)

The variations in the morphology of the bleached and unbleached pulp fibers were examined using a scanning electron microscope JEOL JSM-7000F with field emission cathode, with a lateral resolution of 1.2 nm at 20 kV. The images selected were regarded to be representative of the fiber surfaces. The diameter of cellulose fibers were measured by analyzing SEM images using ImageJ software.

2.6.2. Atomic force microscopy (AFM)

AFM was used to investigate the morphology of CNF and LCNF. AFM images were obtained operating in tapping mode with a scanning probe microscope: Nanoscope IIIa Multimode™ Digital Instruments (Waltham, MA, Spain), equipped with an integrated silicon tip cantilever with a resonance frequency of 300 kHz.

2.6.3. X-ray diffraction (XRD)

The crystallinity of bleached and unbleached CNFs samples was calculated using X-ray diffraction (XRD). The XRD spectra were collected on a Phillips X'Pert PRO automatic diffractometer (Phillips N. V., Amsterdam, Netherlands) operating at 40 kV and 40 mA in the theta-theta configuration. Monochromatic Cu-Kα (λ = 1.5418 Å) radiation and a PIXcel solid-state detector (active length in 2θ = 3.347°) were employed. The samples were recorded over the angular range of 2θ = 5–40° at a scan rate of 2°/min. The crystallinity index (CI) was obtained considering the peak deconvolution method (Park et al., 2010). Individual peaks were extracted assuming Voigt functions by the peak fitting process with a licensed version of PeakFit (4.12). The CI was calculated with Eq. 1:

$$\%\ \ Cristallinity\ \ = \left[\frac{\sum A_{Cr}}{A_T}\right] \times 100 \qquad (1)$$

where A_{Cr} is attributed to the sum of crystalline peaks and A_T to total area.

2.6.4. Differential scanning calorimetry (DSC)

Thermal properties of CNF and LCNF before and after modification were investigated through DSC analyses performed on a Mettler Toledo DSC 822 apparatus (Mettler Toledo, Spain). Around 5 mg of CNFs powders was introduced in aluminum pans and then subjected to a heating ramp from room temperature to 275 °C (10 °C/min) under a nitrogen atmosphere (50 mL/min) to avoid thermo-oxidative reactions. The calibration was performed with indium standard. A first heating-cooling cycle from room temperature to 100 °C (heating rate of 10 °C/min and cooling rate of 20 °C/min) was performed to clear the thermal history of CNFs samples. The thermal transitions were recorded on the second heating-cooling cycle.

2.6.5. Thermogravimetric analysis (TGA)

TGA experiments were completed on a TGA/SDTA 851 Mettler Toledo (Mettler Toledo, Spain) instrument. Around 5 mg of CNFs were introduced in a standard ceramic alumina pan and then subjected to a heating ramp from 30° to 800 °C (10 °C/min) under a nitrogen atmosphere (50 mL/min) to avoid thermo-oxidative reactions. The onset of thermal degradation and the maximum degradation temperatures were determined using DTG curves.

2.6.6. Fourier transform infrared spectroscopy (FTIR)

Fourier transform infrared spectra of native and esterified samples were acquired on a PerkinElmer Spectrum Two FTIR Spectrometer equipped with a Universal Attenuated Total Reflectance accessory using an internal reflection diamond crystal lens to collect Infrared spectra samples. The studied range was from 400 to 4000 cm^{-1}, and the resolution was 8 cm^{-1}. 24 scans were recorded for each dry sample.

2.6.7. Nuclear magnetic resonance (NMR)

Solid-state ^{13}C NMR spectrometry with cross-polarization (CP) and magic-angle spinning (MAS) was performed at room temperature using a Bruker 500 MHz spectrometer at a frequency of 250 MHz with an acquisition time of 0.011 s. Spectra were recorded over 32 scans for all the nanofibers.

3. Results and discussion

The results of this study are organized in two parts. The first part will focus on the characterization of the nanofibers extracted from the bleached and unbleached cellulose pulp. The second part will be dedicated to the characterization of the cellulose nanofibers esterified using an aromatic amine compound.

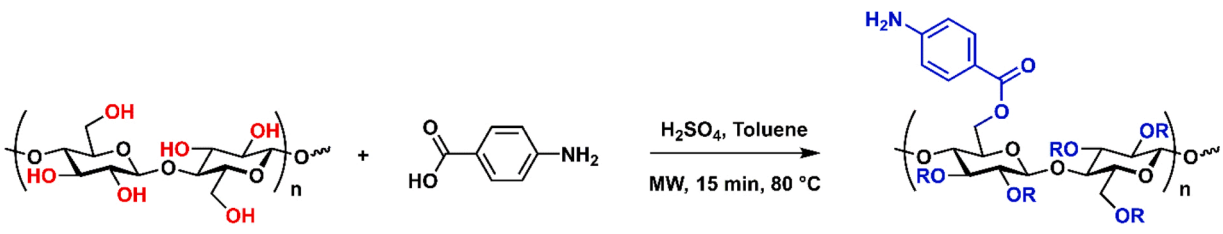

Scheme 1. Microwave assisted esterification of cellulose nanofibers with *para*-aminobenzoic acid.

3.1. Characterization of LCNF and CNF

3.1.1. Chemical composition of the Eucalyptus pulp

The chemical composition of the unbleached and bleached cellulose pulp determined by TAPPI standard methods is listed in Fig. 1. The unbleached pulp is composed of 66.9 % of cellulose, 23.4 % of hemicelluloses, and 7.33 % of lignin, similar to what could be found in the literature (Demuner et al., 2020; Robles et al., 2021). The cellulose, hemicelluloses, and lignin content for the bleached pulp was about 73.3 %, 22.62 %, and 2.33 %, respectively. As expected, for the bleached pulp, the lignin fractions, as well as the extractives and ashes fractions, were lower following the bleaching treatment. The difference between these samples is directly associated with the higher residual lignin content present in the unbleached eucalyptus pulps, therefore demonstrating the efficiency of the bleaching treatment to separate cellulose from other biopolymers.

The FTIR spectra of CNF and LCNF are shown in Fig. S1 (Supplementary materials). It can be appreciated that the spectra have few differences. The few variations are related to phenolic compounds identified as part of the lignin structure. The spectral band located at $\upsilon = 3336\ cm^{-1}$ associated with the aromatic and aliphatic O–H stretching vibrations (Jiang and Hsieh, 2013) shows a slight decrease for the bleached pulp as compared to the unbleached one. A similar effect was observed for the peak located at $\upsilon = 1427\ cm^{-1}$, corresponding to the aromatic C–H deformation vibration of lignin (Chen et al., 2011). It was still observed in the CNF, although the intensity slightly declined. This indicates that a small amount of lignin still exists in the bleached cellulose pulp. Other peaks, i.e., $\upsilon = 1061$ and $897\ cm^{-1}$, associated with the C–O stretching and C_1–H deformation vibrations of cellulose increased in the FTIR spectra of CNF (Alemdar and Sain, 2008).

3.1.2. Morphology of the CNF and LCNF

The morphology of the unbleached and the bleached cellulose fibers was investigated before and after the mechanical fibrillation process. Fig. 2.a and c present SEM images of the unbleached and the bleached pulps. Before fibrillation, both pulps showed a needle-like or rod-like structure formed from the random interweaving of fibers (Henriksson et al., 2008). During the extraction, the unbleached pulp that contains a higher lignin fraction (Fig. 1) exhibits superior resistance to defibrillation. This was manifested by the presence of larger fibers as evidenced by pressure fluctuations and clogging of the homogenizer. At higher magnification, it appears from the SEM images shown in Fig. 2.b and d, that the unbleached fibers present a smooth and homogeneous surface, while the bleached fibers have a rough surface with a tortuous appearance resulting from the bleaching treatment. The SEM images analysis revealed fiber diameters in the range of 12–25 μm for the unbleached pulp, slightly larger than the bleached pulp, which displays fibers with a diameter between 9 and 16 μm. This resulted in a homogenization of the unbleached fibers after additional passes.

AFM topographies of nanofibrillated samples after being exposed to mechanical shear force are shown in Fig. 2.e and Fig. 2.f. These micrographs tend to indicate that both pulps were completely isolated to a nanosize level. It can also be seen that the diameters of the homogenized unbleached (LNCF) and bleached (CNF) nanofibrils were very similar (nearly 23 and 59 nm, respectively). The length of the extracted nanofibrils was estimated to be several micrometers.

Normalized XRD patterns of the CNF and LCNF prepared by mechanical fibrillation are reported in Fig. 3. The spectra show a sharp, high peak at $2\theta = 23.6°$ and the double peak at $2\theta = 16.5°$ are attributed to the cellulose I crystalline domains (Heritage et al., 1963). A broadening of the peaks is observed in the case of LCNF as compared to CNF. This is related to the presence of a lignin-corresponding signal, which usually has a broad and weak diffraction pattern ranging from 10° to 35° (Robles et al., 2021; Gupta et al., 2015). The crystallinity of nanofibers depends on the initial content of the amorphous structure governed by the presence of hemicellulose and lignin produced during the biosynthesis of wood cell walls (Moon et al., 2011). It may also vary due to alterations in cellulose chains during bleaching processes (Lavoine et al., 2012). In the current work, the crystallinity index values (CI) of the LCNF and CNF samples were determined according to Eq. 1, resulting in 60.68 % and 62.51 %, respectively. Comparing CNF and LCNF from the same biomass, the crystallinity index values differ slightly as those previously reported in the literature (Demuner et al., 2020). The higher crystallinity index determined for CNF fibers is originated from the bleaching treatment that eliminates amorphous regions of fibers, notably lignin and hemicelluloses (Walker, 2006); nevertheless, the slight difference implies that the bleaching process does not affect considerably the crystalline structure of the fibers.

3.1.3. Thermal properties of CNF extracted

Thermogravimetric analysis (TGA) was conducted to compare the thermal stability of the nanofibers, a feature influenced by the chemical composition, the crystallinity, and the surface area of the pulps (Skodras et al., 2006). It has been widely reported that the thermal decomposition of cellulosic materials occurs between 200 and 400 °C (Skodras et al., 2006). Degradation occurs in several steps, including water evaporation, followed by polymer decomposition. Fig. 4 displays the TGA curves of LCNF and CNF samples. Table 1 summarizes the T_{onset} and T_{max} of each sample. The first stage of thermal degradation occurred between 100 and 110 °C, which contributed to 3.9 % and 3.5 % of the total weight loss for LCNF and CNF, respectively.

This phenomenon corresponded to the evaporation of water molecules that are physically bonded to the fibers. The second stage of degradation, corresponding to the degradation of the lignocellulosic component, occurs in the range of 250–256 °C. This decomposition starts primarily in the amorphous regions. The onset temperature of degradation (T_{onset}) was observed at 250 and 256 °C, while the maximum degradation (T_{max}) was measured around 333 and 336 °C for

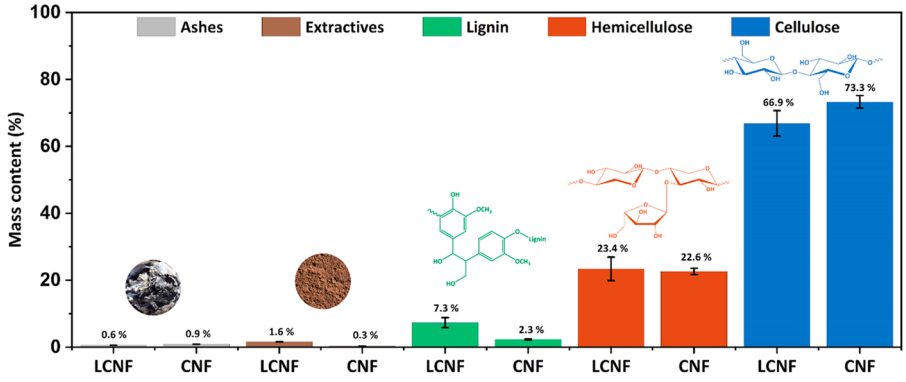

Fig. 1. Chemical composition of the unbleached and bleached cellulose pulp.

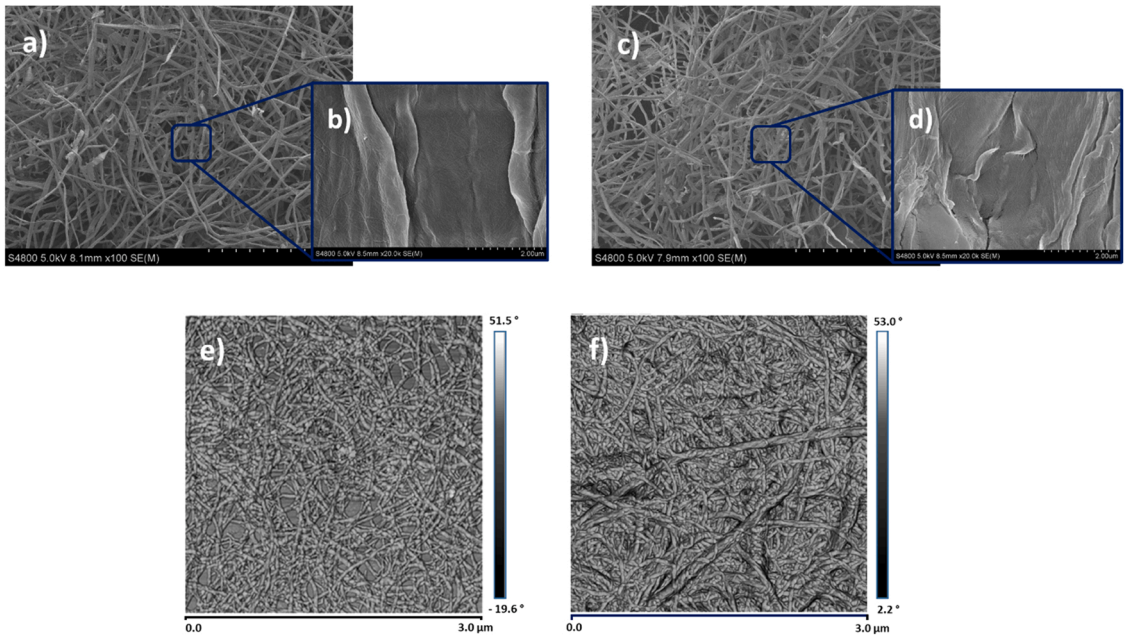

Fig. 2. SEM images of a) unbleached cellulose fibers; b) suface of unbleached cellulose fibers; c) bleached cellulose fibers and d) suface of bleached cellulose fibers. AFM images of the elaborated nanofibers: e) lignocellulose nanofibers (LNCF) and f) cellulose nanofibers (CNF).

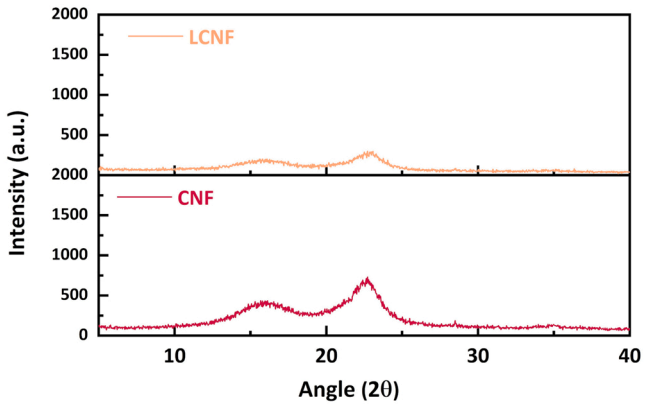

Fig. 3. X-ray diffractograms of LCNF: lignocellulose nanofibers from the unbleached pulp; CNF: cellulose nanofibers from the bleached pulp.

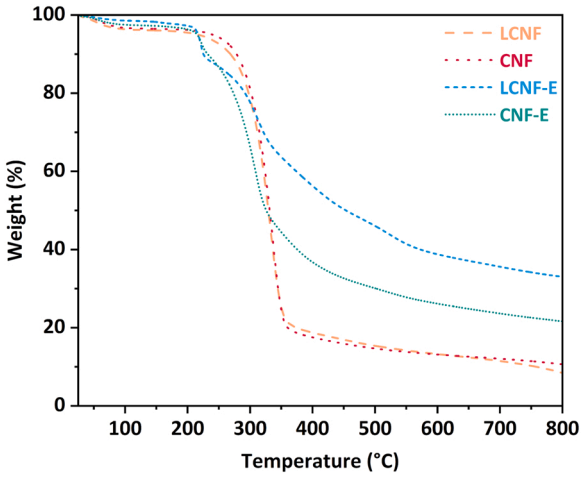

Fig. 4. Thermogravimetry analysis of LCNF: lignocellulose nanofibers from unbleached pulp; CNF: cellulose nanofibers from bleached pulp; LCNF-E: esterified lignocellulose nanofibers; CNF-E: esterified cellulose nanofibers.

LCNF and CNF, respectively. Thus, better thermal resistance is observed in the case of bleached nanofibers (CNF). The removal of lignin after bleaching could explain this better stability of bleached nanofibers . This is also due to a higher degree of crystallinity in bleached nanofibers as previously observed in the XRD analysis. In addition, a higher degree of crystallinity of cellulose may result in a greater heat resistance with a higher temperature of thermal degradation (Jonoobi et al., 2009) Table 1.

3.2. Microwave-assisted esterification of LCNF and CNF

In this section, the potential of MW technology towards the sustainable esterification of cellulose nanofibers with an aromatic amine derivative will be discussed. The esterification of cellulose nanofibers previously extracted from unbleached (LNCF) and bleached (CNF) Eucalyptus pulp was carried out with *para*-aminobenzoic acid in the presence of sulfuric acid and toluene, respectively employed as catalyst and solvent. Toluene is a well-suited solvent for MW reactions as it absorbs microwave irradiation and heats up rapidly. One main advantage of microwave irradiation is the significant decrease in reaction time from several hours for conventional esterification to several minutes reported here.

The formation of the esterified CNF can be confirmed in the FTIR spectra. The spectra of neat and modified CNFs are shown in Fig. 5. The different peaks of the neat nanofibers were attributed in the previous part. It can be observed that the band at $\upsilon = 3336\ cm^{-1}$, which corresponds to the hydroxyl group on the surface of the nanofibrils, has slightly decrease in the spectrum of nanofibers LCNF-E and CNF-E after esterification, giving way to the emergence of new peaks. The appearance of the stretching band at $\upsilon = 1695\ cm^{-1}$ is associated with carbonyl connected to the aromatic group (Sharma et al., 2016). The presence of this band indicated the formation of acetyl groups resulting from the acetylation of hydroxyl groups. Other characteristic absorption bands have been observed, including a band of C-C stretching vibrations in the aromatic ring ($\upsilon = 1612\ cm^{-1}$), asymmetric stretching vibrations of C-N-C ($\upsilon = 1122\ cm^{-1}$), and a bimodal band centered at $\upsilon = 851\ cm^{-1}$ associated with the out-of-plane bending vibrations of C-H bond

Table 1
Thermal proprerties of LCNF: lignocellulose nanofibers from unbleached pulp; CNF: nanofibers from bleached pulp; LCNF-E: esterified lignocellulose nanofibers; CNF-E: esterified bleached nanofibers.

Sample	H_2O content (%)[a]	T_{onset} (°C)[b]	$T_{d5\%}$ (°C)[c]	$T_{max,1}$ (°C)[d]	$T_{max,2}$ (°C)[e]	Char (%)[f]	LOI (%)[g]
LCNF	3.9	250	217	n.a.	333	8.4	20.9
CNF	3.5	256	240	n.a.	336	10.6	21.8
LCNF-E	2.8	203	217	222	314	33.0	30.7
CNF-E	1.8	205	216	223	309	21.7	26.2

T_{onset}: the onset temperature of degradation; T_{max}: the maximum temperature of the main degradation stage; LOI: low oxygen index. n.a: no applicable.
[a] determined from the first derivative (Fig. S3, Supporting information),
[b] determined from the first derivative (Fig. S3, Supporting information),
[c] major degradation temperature (Fig. S4, Supporting information),
[d] major degradation temperature (Fig. S4, Supporting information),
[e] major degradation temperature (Fig. S4, Supporting information),
[f] CR at 800 °C,
[g] calculated according the equation of Krevelen 2022.

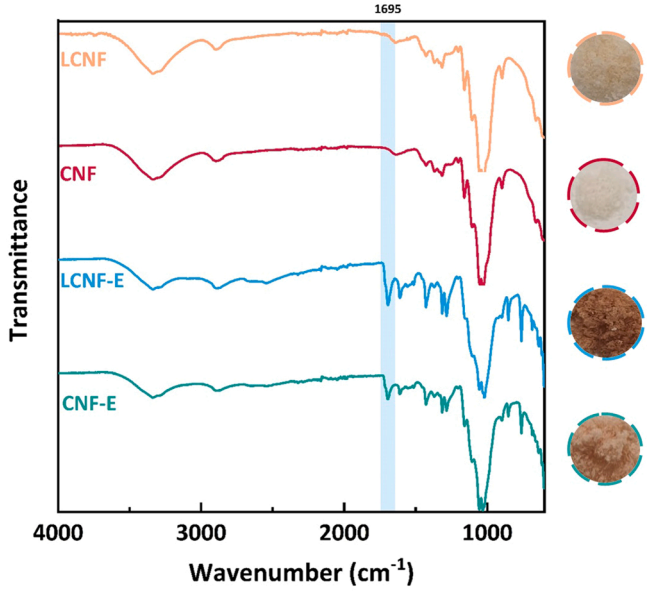

Fig. 5. FTIR spectra of LCNF: lignocellulose nanofibers from unbleached pulp; CNF: nanofibers from bleached pulp; LCNF-E: esterified lignocellulose nanofibers ; CNF-E: esterified cellulose nanofibers .

respectively (Lochab, 2014). However, it can be observed that the band corresponding to the ester is more intense in the case of LCNF-E than that present on the CNF-E spectrum. This seems to be in line with the observations made earlier. Indeed, it was observed that nanofibers that did not undergo bleaching (LCNF) showed an increase in the band corresponding to the free hydroxyl group (υ= 3336 cm^{-1}).

The ^{13}C NMR spectrum reported in Fig. 6 also confirms the successful esterification of cellulose nanofibers. The ^{13}C NMR spectrum of the native CNF showed typical cellulose carbon peaks C1, C4, C2-C3-C5, and C6 respectively observed at δ = : 105, 89, 70–80, and 65.3 ppm, respectively. For the esterified CNFs, several new peaks appear on the spectra. The peak centered at δ = 170 ppm was assigned to the carbonyl ester bond. Both esterified samples (LCNF-E and CNF-E) also showed new signals in the aromatic area (115–165 ppm) corresponding to the aromatic part of the *para*-aminobenzoic acid (a, b, c, d, and e) (El-Obeid and Al-Badr, 1993).

In addition to the structural modifications, the physicochemical properties of the esterified CNFs were altered as confirmed by DSC

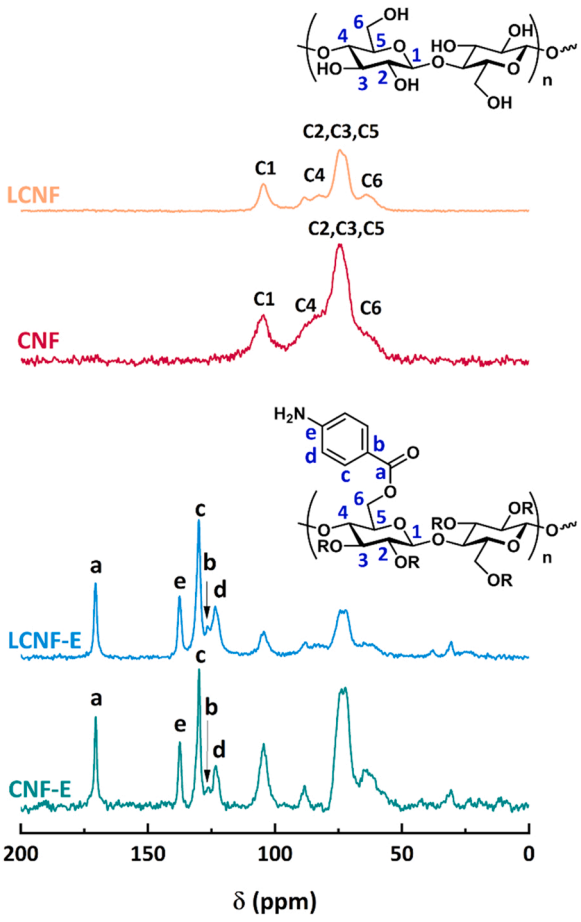

Fig. 6. ^{13}C NMR spectrum of LCNF: lignocellulose nanofibers from unbleached pulp; CNF: nanofibres from bleached pulp; LCNF-E: esterified lignocellulose nanofibers; CNF-E: esterified cellulose nanofibers.

analysis. The DSC curves of LCNF and CNF before and after chemical modifications are shown in Fig. 7. The parameters analyzed during the heating stage (T_m, ΔH_m) are summarized in Table 2. The spectra of pristine nanofibers (CNF and LCNF) present a single endothermic shift around T = 100 °C caused by the gradual evaporation of water adsorbed by the fibers, although they have been dried at T = 50 °C for 48 h before

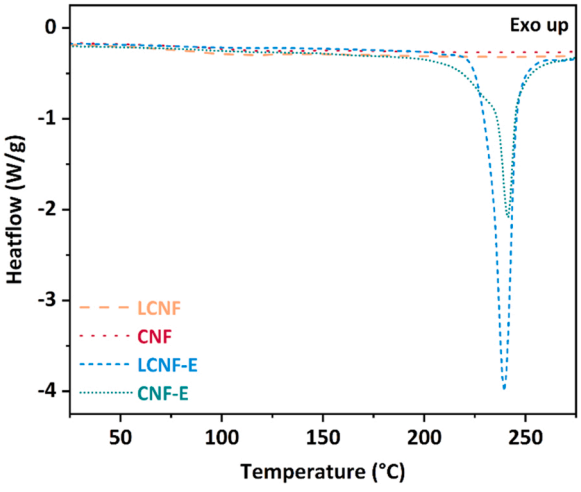

Fig. 7. DSC spectrum of LCNF: lignocellulose nanofibers from unbleached pulp; CNF: nanofibers from bleached pulp; LCNF-E: esterified lignocellulose nanofibers; CNF-E: esterified bleached nanofibers.

Table 2
DSC results of LCNF: lignocellulose nanofibers from unbleached pulp; CNF: nanofibers from bleached pulp; LCNF-E: esterified lignocellulose nanofibers; CNF-E: esterified cellulose nanofibers.

Sample	Δm_1 (J/g)[a]	T_{m1} (°C)[b]	Δm_2 (J/g)[c]	T_{m2} (°C)[d]
LCNF	- 61.2	103	n.a	n.a.
CNF	- 44.7	107	n.a	n.a.
LCNF-E	- 17.4	108	- 132.7	242
CNF-E	- 22.7	106	- 229.5	243

n.a: no applicable.
[a] Enthalpy of the first endotherm by DSC (N_2, 10 °C.min^{-1}),
[b] Maximum temperature of the first melting endotherm by DSC (N_2, 10 °C.min^{-1}),
[c] Enthalpy of the second endotherm by DSC (N_2, 10 °C.min^{-1}),
[d] Maximum temperature of the second melting endotherm by DSC (N_2, 10 °C.min^{-1}),

analysis. Cellulose has a strong affinity for hydroxyl-bearing systems, specifically for small molecules as water aggregates adsorb to the external surface of microfibrils. Therefore, the more hydroxyl groups the fibers have on the surface, the higher the water content. Therefore, it can be observed that the amount adsorbed by LCNF is more important than that of CNF. The latest result agrees with the observations made by FTIR analysis, where a more intense peak of hydroxyl groups was observed in the LCNF sample.

Two peaks were observed for the esterified nanofibers (LCNF-E and CNF-E). The first endothermic shift is located at T = 106 °C, which corresponds to the evaporation of the adsorbed water molecules, as in the case of pristine fibers. Interestingly, the molar enthalpy (Δm) was found to decrease compared to that of pristine fibers (LCNF and CNF). This decrease resulting from the hydroxyl groups's esterification present on the cellulose's nanofibers surface. Therefore, the second exothermic peak observed in the DSC spectrum may correspond to the thermal degradation of the aromatic ester bond. This assumption was verified in the following paragraph by TGA analysis. In addition, the molar enthalpy associated with this second exothermic peak was found to be higher in the case of LCNF-E, which can be again credited to the higher numbers of free hydroxyl groups on the surface of pristine LCNF.

The thermal decomposition of the neat nanofibers (CNF and LCNF) and the esterified nanofibers (LCNF-E and CNF-E) was investigated via TGA. The spectra of samples are shown in Fig. 4. As detailed above, a two-stage degradation pattern was observed for the thermal degradation of the pristine nanofibers, with first the evaporation of moisture followed by the decomposition of the chemical structure occurring around T = 300 °C. On the other hand, the esterified nanofiber (LCNF-E and CNF-E) follows a three-stage degradation pattern, starting from the dehydration of aliphatic —OH groups, followed by the interunit linkages cleavage, and terminated with the decomposition of the polymer. The onset temperature of degradation (T_{onset}) determined from the first derivative of the TGA curve (DTG), the maximum temperature of the main degradation stage (T_{max}), and the char residue are summarized in Table 1. Compared to the pristine nanofibers, the thermal properties of the esterified nanofibers display a lower T_{onset} attributed to the lower degree of crystallinity in nanofibers after acetylation (Fig. S4 in Supplementary materials). In addition, the partial substitution of hydroxyl groups can decrease the density of hydrogen bonding between the cellulose molecules during the acetylation, thus partially destroying cellulose nanofibers crystalline structure. Concerning char, it increased significantly after esterification (from 8.4 % to 33 % for LCNF) due to the formation of the aromatic ester. This also increased the low oxygen content index (LOI) from 20.9 % to 30.7 %, indicating improved flame retardant behavior.

4. Conclusions

LCNF and CNF were successfully extracted from Eucalyptus cellulose pulp through the homogenization process, then chemically modified using *para*-aminobenzoic acid under microwave irradiation. CNFs with diameters ranging from 23 to 59 nm and lengths reaching few microns were obtained. A higher crystallinity index was obtained for CNF and LCNF samples. Microwave-assisted esterification of the extracted nanofibers was successfully performed. The chemical modification of cellulose's hydroxyl groups was further confirmed by solid-state ^{13}C NMR and FTIR spectroscopy. XRD and TGA were used to identify the effect of the esterification on the crystallinity and thermal properties of the CNFs. The esterified CNFs showed increased thermal stability regarding the maximum temperature of thermal degradation and higher char yield. The results collected from the various analyses indicate that the method used for the esterification occurred in the amorphous and crystalline parts of the cellulose nanofibers. Finally, the esterified nanofibers prepared from an abundant biopolymer and a biologically produced carboxylic acid represent a sustainable precursor for the production of highly functional bio-based materials. Further assays aiming to assert the effect of reaction conditions to tune the extent of esterification achieved in CNF are currently in progress. These tests will allow us to have highly regioselective esterification of nanofibers without compromising their crystalline structure.

CRediT authorship contribution statement

Farida Baraka: Data curation, Formal analysis, Writing – original draft, Writing – review & editing. **Eduardo Robles:** Supervision, Methodology. **Jalel Labidi:** Funding acquisition, Investigation, Project administration, Resources, Supervision, Validation, Writing – review & editing.

Declaration of Competing Interest

The authors declare that they have no known competing financial interests or personal relationships that could have appeared to influence the work reported in this paper.

Data availability

Data will be made available on request.

Acknowledgments

The authors wish to acknowledge financial support of the Basque Government (IT1498-22) and the University of the Basque Country (PIF21/52 and COLAB20/04). E.R. wants to acknowledge the tenure track position "Bois: Biobased materials" part of E2S UPPA supported by the "Investissements d'Avenir" French program managed by ANR [ANR-16-IDEX-0002]. The authors would like to acknowledge the technical and human assistance received from SGIker [UPV/ EHU/ERDF, EU], Spain. The authors would also like to thank Antoine Adjaoud for the scientific discussion.

Declaration of Competing Interest

We have no conflicts of interest to disclose.

Appendix A. Supporting information

Supplementary data associated with this article can be found in the online version at doi:10.1016/j.indcrop.2022.115970.

References

Alemdar, A., Sain, M., 2008. Isolation and characterization of nanofibers from agricultural residues – wheat straw and soy hulls. Bioresour. Technol. 99 (6), 1664–1671. https://doi.org/10.1016/j.biortech.2007.04.029.

Aloulou, F., Boufi, S., Labidi, J., 2006. Modified cellulose fibres for adsorption of organic compound in aqueous solution. Sep. Purif. Technol. 52 (2), 332–342. https://doi.org/10.1016/j.seppur.2006.05.008.

Bian, H., Gao, Y., Wang, R., Liu, Z., Wu, W., Dai, H., 2018. Contribution of lignin to the surface structure and physical performance of cellulose nanofibrils film. Cellulose 25 (2), 1309–1318. https://doi.org/10.1007/s10570-018-1658-x.

Bouhdadi, R., Benhadi, S., Molina, S., George, B., El Moussaouiti, M., Merlin, A., 2011. Chemical modification of cellulose by acylation: application to adsorption of Methylene blue. Cienc. Y. Tecnol. 13 (1), 105–116. https://doi.org/10.4067/S0718-221×2011000100009.

Chang, C., Hou, J., Chang, P., & Huang, J. , 2019. Structure and properties of cellulose nanocrystals. In Nanocellulose: From Fundamentals to Advanced Materials (p. 21–52); John Wiley & Sons, Ltd.: Hoboken, NJ, USA, 2019; pp. 21–52. ISBN 978-3-527-80743-7.

Chen, W., Yu, H., Liu, Y., Chen, P., Zhang, M., Hai, Y., 2011. Individualization of cellulose nanofibers from wood using high-intensity ultrasonication combined with chemical pretreatments. Carbohydr. Polym. 83 (4), 1804–1811. https://doi.org/10.1016/j.carbpol.2010.10.040.

Chhajed, M., Yadav, C., Agrawal, A., Maji, P., 2019. Esterified superhydrophobic nanofibrillated cellulose based aerogel for oil spill treatment. Carbohydr. Polym. 226, 115286 https://doi.org/10.1016/j.carbpol.2019.115286.

Demuner, I., Colodette, J., Gomes, F., Oliveira, R., 2020. Study of LCNF and CNF from pine and eucalyptus pulps. Nord. Pulp Pap. Res. J. 35 (4), 670–684. https://doi.org/10.1515/npprj-2019-0075.

Eichhorn, S., Dufresne, A., Aranguren, M., Marcovich, N., Capadona, J., Rowan, S., Weder, C., Thielemans, W., Roman, M., Renneckar, S., Gindl, W., Veigel, S., Keckes, J., Yano, H., Abe, K., Nogi, M., Nakagaito, A., Mangalam, A., Simonsen, J., Peijs, T., 2010. Review: current international research into cellulose nanofibres and nanocomposites. J. Mater. Sci. 45 (1), 1–33. https://doi.org/10.1007/s10853-009-3874-0.

El-Obeid, H., & Al-Badr, A. (1993). Aminobenzoic Acid. In Analytical Profiles of Drug Substances and Excipients (Harry G. Brittain, Vol. 22, p. 33–106).

Eyholzer, C., Tingaut, P., Zimmermann, T., Oksman, K., 2012. Dispersion and reinforcing potential of carboxymethylated nanofibrillated cellulose powders modified with 1-hexanol in extruded poly(Lactic Acid) (PLA) Composites. J. Polym. Environ. 20 (4), 1052–1062. https://doi.org/10.1007/s10924-012-0508-4.

Gupta, A., Mohanty, S., Nayak, S., 2015. Preparation and characterization of lignin nanofibre by electrospinnig technique. Int. J. Sci. Eng. Appl. Sci. 1 (3), 184–190.

Henriksson, M., Berglund, L., Isaksson, P., Lindström, T., Nishino, T., 2008. Cellulose nanopaper structures of high toughness. Biomacromolecules 9 (6), 1579–1585. https://doi.org/10.1021/bm800038n.

Her, K., Jeon, S., Lee, S., Shim, B., 2020. Esterification of cellulose nanofibers with valeric acid and hexanoic acid. Macromol. Res. 28 (12), 1055–1063. https://doi.org/10.1007/s13233-020-8146-5.

Heritage, K., Mann, J., Roldan-Gonzalez, L., 1963. Crystallinity and the structure of celluloses. J. Polym. Sci. Part A: Gen. Pap. 1 (2), 671–685. https://doi.org/10.1002/pol.1963.100010208.

Herrick, F.W., Casebier, R.L., Hamilton, J.K., Sandberg, K.R., 1983. Microfibrillated cellulose: morphology and accessibility. J. Appl. Polym. Sci. Appl. Polym. Symp. 37–9, 797–813.

Jiang, F., Hsieh, Y.-L., 2013. Chemically and mechanically isolated nanocellulose and their self-assembled structures. Carbohydr. Polym. 95 (1), 32–40. https://doi.org/10.1016/j.carbpol.2013.02.022.

Joly, C., Verneuil, B., Branland, P., Granet, R., Krausz, P., Rozier, J., Petit, C., 2002. Rapid homogenous esterification of cellulose induced by microwave irradiation. Carbohydr. Polym. 49 (3), 373–376. https://doi.org/10.1016/S0144-8617(02)00004-8.

Jonoobi, M., Harun, J., Shakeri, A., Misra, M., Oksmand, K., 2009. Chemical composition, crystallinity, and thermal degradation of bleached and unbleached kenaf bast (Hibiscus cannabinus) pulp and nanofibers. Bioresources 4 (2), 626–639.

Lavoine, N., Desloges, I., Dufresne, A., Bras, J., 2012. Microfibrillated cellulose – its barrier properties and applications in cellulosic materials: a review. Carbohydr. Polym. 90 (2), 735–764. https://doi.org/10.1016/j.carbpol.2012.05.026.

Li, J., Wang, Y., Wei, X., Wang, F., Han, D., Wang, Q., Kong, L., 2014. Homogeneous isolation of nanocelluloses by controlling the shearing force and pressure in microenvironment. Carbohydr. Polym. 113, 388–393. https://doi.org/10.1016/j.carbpol.2014.06.085.

Li, W., Zhao, X., Huang, Z., Liu, S., 2013. Nanocellulose fibrils isolated from BHKP using ultrasonication and their reinforcing properties in transparent poly (vinyl alcohol) films. J. Polym. Res. 20 (8) https://doi.org/10.1007/s10965-013-0210-9.

Lochab, B., 2014. Naturally occurring phenolic sources: monomers and polymers. RSC Adv. 4 (42), 21712–21752. https://doi.org/10.1039/C4RA00181H.

Lönnberg, H., Fogelström, L., Berglund, L., Malmström, E., Hult, A., 2008. Surface grafting of microfibrillated cellulose with poly(ε-caprolactone) – Synthesis and characterization. Eur. Polym. J. 44 (9), 2991–2997. https://doi.org/10.1016/j.eurpolymj.2008.06.023.

Menon, M.P., Selvakumar, R., Ramakrishna, S., Sureshkumar, P., 2017. Extraction and modification of cellulose nanofibers derived from biomass for environmental application. RSC Adv. 7 (68), 42750–42773. https://doi.org/10.1039/C7RA06713E.

Missoum, K., Belgacem, N., Bras, J., 2013. Nanofibrillated cellulose surface modification: a review. Materials 6 (5), 1745–1766. https://doi.org/10.3390/ma6051745.

Moon, R.J., Martini, A., Nairn, J., Simonsen, J., Youngblood, J., 2011. Cellulose nanomaterials review: structure, properties and nanocomposites. Chem. Soc. Rev. 40 (7), 3941–3994. https://doi.org/10.1039/c0cs00108b.

Nair, S., Zhu, J.Y., Yulin, D., Ragauskas, A., 2014. Charaterization of cellulose nanofibrillation by micro grinding. J. Nanopart. Res. 16 (4), 1–10. https://doi.org/10.1007/s11051-014-2349-7.

Nooy, A.E.J., Besemer, A., Bekkum, H., 2010. Highly selective TEMPO mediated oxidation of primary alcohol groups in polysaccharides. Recl. Des. Trav. Chim. Des. 113 (3), 165–166. https://doi.org/10.1002/recl.19941130307.

Oliveira, R., Colodette, J., Eiras, K., Ventorim, G., 2006. The effect of wood supply and bleaching process on pulp brightness stability. Rev. Árvore 30 (3), 439–450. https://doi.org/10.1590/S0100-67622006000300014.

Park, S., Baker, J., Himmel, M., Parilla, P., Johnson, D., 2010. Cellulose crystallinity index: measurement techniques and their impact on interpreting cellulase performance. Biotechnol. Biofuels 3 (1). https://doi.org/10.1186/1754-6834-3-10.

Ragab, S., El Nemr, A., 2018. Nanofiber cellulose di- and tri-acetate using ferric chloride as a catalyst promoting highly efficient synthesis under microwave irradiation. J. Macromol. Sci., Part A 55 (2), 124–134. https://doi.org/10.1080/10601325.2017.1387741.

Ramírez, J., Suriano, C., Cerrutti, P., Foresti, L., 2014. Surface esterification of cellulose nanofibers by a simple organocatalytic methodology. Carbohydr. Polym. 114, 416–423. https://doi.org/10.1016/j.carbpol.2014.08.020.

Robles, E., Csóka, L., Labidi, J., 2018. Effect of reaction conditions on the surface modification of cellulose nanofibrils with aminopropyl triethoxysilane. Coatings 8 (4), 139. https://doi.org/10.3390/coatings8040139.

Robles, E., Izaguirre, N., Martin, A., Moschou, D., Labidi, J., 2021. Assessment of bleached and unbleached nanofibers from pistachio shells for nanopaper making. Molecules 26 (5), 1371. https://doi.org/10.3390/molecules26051371.

Rojo, E., Peresin, M., Sampson, W., Hoeger, I., Vartiainen, J., Laine, J., Rojas, O., 2015. Comprehensive elucidation of the effect of residual lignin on the physical, barrier, mechanical and surface properties of nanocellulose films. Green Chem. 17 (3), 1853–1866. https://doi.org/10.1039/C4GC02398F.

Sehaqui, H., Kulasinski, K., Pfenninger, N., Zimmermann, T., Tingaut, P., 2016. Highly Carboxylated Cellulose Nanofibers via Succinic Anhydride Esterification of Wheat Fibers and Facile Mechanical Disintegration. Biomacromolecules 18 (1), 242–248. https://doi.org/10.1021/acs.biomac.6b01548.

Semsarilar, M., Perrier, S., 2009. Solubilization and functionalization of cellulose assisted by microwave irradiation. Aust. J. Chem. 62 (3), 223–226. https://doi.org/10.1071/CH08491.

Sharma, P., Kumar, D., Roy, P., 2016. Microwave-assisted sustainable synthesis of telechelic poly(ethylene glycol)s with benzoxazine end groups. ChemistrySelect 1 (21), 6941–6947. https://doi.org/10.1002/slct.201601226.

Singh, M., Kaushik, A., Ahuja, D., 2016. Surface functionalization of nanofibrillated cellulose extracted from wheat straw: effect of process parameters. Carbohydr. Polym. 150, 48–56. https://doi.org/10.1016/j.carbpol.2016.04.109.

Skodras, G., Panagiotis, G., Basinas, P., Kakaras, E., Sakellaropoulos, G., 2006. Pyrolysis and combustion characteristics of biomass and waste-derived feedstock. Ind. Eng. Chem. Res. 45 (11), 3791–3799. https://doi.org/10.1021/ie060107g.

Spence, K., Venditti, R., Rojas, O., Habibi, Y., Pawlak, J., 2010. The effect of chemical composition on microfibrillar cellulose films from wood pulps: water interactions and physical properties for packaging applications. Cellulose 17 (4), 835–848. https://doi.org/10.1007/s10570-010-9424-8.

Turbak, A.F., Snyder, F.W., & Sandberg, K.R. , 1983. Microfibrillated cellulose (Patent N° US4374702A).

Vartiainen, J., Pöhler, T., Sirola, K., Pylkkanen, L., Alenius, H., Hokkinen, J., Tapper, U., Lahtinen, P., Kapanen, A., Putkisto, K., Hiekkataipale, P., Eronen, P., Ruokolainen, J., Laukkanen, A., 2011. Health and environmental safety aspects of friction grinding and spray drying of microfibrillated cellulose. Cellulose 18 (3), 775–786. https://doi.org/10.1007/s10570-011-9501-7.

Walker, J.C.F., 2006. Primary Wood Processing: Principles and Practice. Springer.

Wang, H., Zhang, X., Jiang, Z., Yu, Z., Yu, Y., 2015. Isolating nanocellulose fibrills from bamboo parenchymal cells with high intensity ultrasonication. Holzforschung 70 (5), 401–409. https://doi.org/10.1515/hf-2015-0114.

Xiang, Z., Gao, W., Chen, L., Lan, W., Zhu, J.Y., Runge, T., 2016. A comparison of cellulose nanofibrils produced from Cladophora glomerata algae and bleached eucalyptus pulp. Cellulose 23 (1), 493–503. https://doi.org/10.1007/s10570-015-0840-7.

Yuan, T., Zeng, J., Wang, B., Cheng, Z., Chen, K., 2021. Cellulosic fiber: mechanical fibrillation-morphology-rheology relationships. Cellulose 28 (12), 7651–7662. https://doi.org/10.1007/s10570-021-04034-y.